

## Pulsed chemical vapor deposition of Cu<sub>2</sub>S into a porous TiO<sub>2</sub> matrix

I. Carbone, Q. Zhou, B. Vollbrecht, L. Yang, S. Medling, A. Bezryadina, F. Bridges, G. B. Alers, J. T. Norman, and T. Kinmen

Citation: *Journal of Vacuum Science & Technology A* **29**, 051505 (2011); doi: 10.1116/1.3609772

View online: <http://dx.doi.org/10.1116/1.3609772>

View Table of Contents: <http://scitation.aip.org/content/avs/journal/jvsta/29/5?ver=pdfcov>

Published by the AVS: Science & Technology of Materials, Interfaces, and Processing

### Articles you may be interested in

Highly conformal magnesium oxide thin films by low-temperature chemical vapor deposition from Mg(H<sub>3</sub>BNMe<sub>2</sub>BH<sub>3</sub>)<sub>2</sub> and water

Appl. Phys. Lett. **102**, 101605 (2013); 10.1063/1.4795860

Experimental and theoretical investigation of the electronic structure of Cu<sub>2</sub>O and CuO thin films on Cu(110) using x-ray photoelectron and absorption spectroscopy

J. Chem. Phys. **138**, 024704 (2013); 10.1063/1.4773583

Chemical nature of colossal dielectric constant of Ca Cu<sub>3</sub> Ti<sub>4</sub> O<sub>12</sub> thin film by pulsed laser deposition

Appl. Phys. Lett. **92**, 172909 (2008); 10.1063/1.2919076

CVD Cu<sub>2</sub>O and CuO Nanosystems Characterized by XPS

Surf. Sci. Spectra **14**, 41 (2007); 10.1116/11.20080701

Nanocrystalline p-type transparent Cu–Al–O semiconductor prepared by chemical-vapor deposition with Cu(acac)<sub>2</sub> and Al(acac)<sub>3</sub> precursors

Appl. Phys. Lett. **76**, 3959 (2000); 10.1063/1.126834



## Instruments for Advanced Science

<p>Contact Hiden Analytical for further details:  <b>W</b> <a href="http://www.HidenAnalytical.com">www.HidenAnalytical.com</a>  <b>E</b> <a href="mailto:info@hiden.co.uk">info@hiden.co.uk</a></p> <p><a href="#">CLICK TO VIEW</a> our product catalogue</p>	 <p><b>Gas Analysis</b></p> <ul style="list-style-type: none"> <li>› dynamic measurement of reaction gas streams</li> <li>› catalysis and thermal analysis</li> <li>› molecular beam studies</li> <li>› dissolved species probes</li> <li>› fermentation, environmental and ecological studies</li> </ul>	 <p><b>Surface Science</b></p> <ul style="list-style-type: none"> <li>› UHV TPD</li> <li>› SIMS</li> <li>› end point detection in ion beam etch</li> <li>› elemental imaging - surface mapping</li> </ul>	 <p><b>Plasma Diagnostics</b></p> <ul style="list-style-type: none"> <li>› plasma source characterization</li> <li>› etch and deposition process reaction</li> <li>› kinetic studies</li> <li>› analysis of neutral and radical species</li> </ul>	 <p><b>Vacuum Analysis</b></p> <ul style="list-style-type: none"> <li>› partial pressure measurement and control of process gases</li> <li>› reactive sputter process control</li> <li>› vacuum diagnostics</li> <li>› vacuum coating process monitoring</li> </ul>
---	--	--	--	--

# Pulsed chemical vapor deposition of Cu<sub>2</sub>S into a porous TiO<sub>2</sub> matrix

I. Carbone, Q. Zhou, B. Vollbrecht, L. Yang, S. Medling, A. Bezryadina, F. Bridges, and G. B. Alers<sup>a)</sup>

*Department of Physics, University of California at Santa Cruz, 1156 High St., Santa Cruz, California 95064*

J. T. Norman

*Air Products Inc., 1969 Palomar Oaks Way, Carlsbad, California 92011*

T. Kinmen

*Department of Physics, Colorado School of Mines, 1500 Illinois St., Golden, Colorado 80401*

(Received 27 February 2011; accepted 24 May 2011; published 27 July 2011)

Chalcocite (Cu<sub>2</sub>S) has been deposited via pulsed chemical vapor deposition (PCVD) into a porous TiO<sub>2</sub> matrix using hydrogen sulfide and a metal-organic precursor. The precursor used is similar to the more common Cu(hfac)(tmvs) precursor, but it is fluorine free and exhibits increased thermal stability. The simultaneous exposure of the substrate to the copper precursor and hydrogen sulfide resulted in nonuniform Cu<sub>2</sub>S films with a temperature independent deposition rate implying gas phase reaction kinetics. The exposure of mesoporous TiO<sub>2</sub> and planar ZnO to alternating cycles of the copper precursor and hydrogen sulfide resulted in a PCVD film that penetrated fully into the porous TiO<sub>2</sub> layer with a constant deposition rate of 0.08 nm/cycle over a temperature range of 150–400 °C. The chalcocite (Cu<sub>2</sub>S) stoichiometry was confirmed with extended x-ray absorption fine structure measurements (EXAFS) and x-ray photoelectron spectroscopy. Calculations of the EXAFS spectrum for different Cu<sub>x</sub>S phases show that EXAFS is sensitive to the different phase stoichiometries. Optical absorption measurements of CVD thin films using photothermal deflection spectroscopy show the presence of a metallic copper-poor phase for gas phase nucleated films less than 100 nm thick and a copper-rich semiconducting phase for thicknesses greater than 100 nm with a direct band gap of 1.8 eV and an indirect bandgap of 1.2 eV. © 2011 American Vacuum Society. [DOI: 10.1116/1.3609772]

## I. INTRODUCTION

The extremely thin absorber (ETA) cell is a solar cell concept that utilizes a highly structured heterojunction to scatter light, thus increasing the effective thickness of the absorbing layer.<sup>1</sup> By allowing for thinner absorbing layers, these devices also reduce the transport path for excited charge carriers. A challenge in the development of solid state ETA devices is finding an effective technique for the deposition of semiconducting materials within nanoporous structures to form an interpenetrating junction. Chemical vapor deposition (CVD) is a gas-phase deposition process that can penetrate into pores as small as 4 nm in diameter,<sup>2</sup> making it a promising technique for fabricating ETA solar cells. This article characterizes Cu<sub>x</sub>S films deposited via pulsed chemical vapor deposition (PCVD) on porous nanocrystalline TiO<sub>2</sub> and planar ZnO for future applications in photovoltaics.

Cu<sub>2</sub>S was a leading thin-film solar cell material in the 1980s due to its indirect band gap near 1.2 eV and its relative abundance and nontoxicity. Cu<sub>2</sub>S/CdS devices achieved an efficiency of 9.1%.<sup>3</sup> However, the diffusion of copper ions across the Cu<sub>2</sub>S/CdS boundary severely limits the lifetime of this device structure.<sup>4</sup> Porous nanocrystalline TiO<sub>2</sub> has been established as an effective dye sensitized solar cell material. In addition, TiO<sub>2</sub> exhibits superior chemical stability and is

expected to form a robust junction when paired with Cu<sub>2</sub>S.<sup>5,6</sup> ZnO is another stable semiconductor that has also been proposed as a window layer material in Cu<sub>2</sub>S devices. Theoretical work has shown that Cu<sub>2</sub>S/ZnO devices should have higher open circuit voltages and collection efficiencies than comparable Cu<sub>2</sub>S/CdS devices.<sup>7</sup>

PCVD is a variant of CVD in which substrates under vacuum are exposed to gaseous precursors containing the constituents of a desired deposition product. A chemical reaction is initiated at or near the substrate's surface, producing the desired material on the substrate. Unlike CVD, PCVD uses a stepwise injection process in which the substrate is separately exposed to each precursor in a series of pulses and purges inside a deposition chamber. PCVD is analogous to atomic layer deposition (ALD) except for the fact that the purge steps are relatively short and it is possible that the reaction chamber still contains gaseous precursor after the purge steps. If the purge steps completely removed all excess precursor, leaving only the chemisorbed species, then this process would be ALD. For PCVD, a single exposure cycle results in the precursor-limited deposition of material that can still be highly conformal, film thickness is determined by the number of cycles used in the process. For all CVD processes, the morphology of the deposited material is largely affected by the nature of the chemical reaction, the conditions inside the deposition chamber, and the surface chemistry of the substrate.

<sup>a)</sup>Corresponding author; electronic email: galers@ucsc.edu

Copper sulfides are known to have at least eight stoichiometric phases ranging from copper-rich Cu<sub>2</sub>S (chalcocite) to copper-poor CuS (covellite).<sup>8,9</sup> Aside from the chalcocite phase, these crystal phases are too conductive to be used as absorbing layers in solar cell devices. Previous work using ALD and Cu(thd)<sub>2</sub> as the copper precursor yielded Cu<sub>1.8</sub>S and CuS, with the phase of the deposited material determined by the substrate temperature during the deposition.<sup>10–12</sup> Other ALD work successfully produced Cu<sub>2</sub>S using bis(N, N'-di-sec-butylacetamidinato)dicopper(I) as the copper precursor.<sup>13</sup> In this article, KI5 was utilized for the fabrication of Cu<sub>x</sub>S materials. KI5 has previously used for the deposition of copper. KI5 is a fluorine-free molecule based on the common Cu(hfac)(tmvs) precursor also known as CupraSelect<sup>®</sup>.<sup>14</sup> The chemical structure of KI5 contains a seven member ring that imparts greater thermal stability, allowing for high vapor pressures (> 2 Torr at 140 °C) and deep penetration into highly structured surfaces.<sup>14</sup> In addition, this precursor avoids fluorine impurities resulting from precursor decomposition.

## II. EXPERIMENT

A custom built reactor was used for the deposition of Cu<sub>x</sub>S. The reactor was a single wafer chamber with two separately controlled injectors used to introduce KI5 and hydrogen sulfide either simultaneously for CVD deposition or as alternating pulses for PCVD deposition. The reaction zone was confined in a “parallel plate” configuration between a 200 mm heated substrate chuck and a 200 mm heated shield 20 mm above the substrate chuck. The copper precursor was heated to 90 °C, and all gas lines between the reactor, injectors, and heat shield were heated to temperatures in the range of 90–100 °C. Outside of the reaction zone was a second shield at ambient temperature. The substrates were 1 in. square substrates placed directly under the injectors. The chamber base pressure prior to deposition was  $\sim 10^{-6}$  Torr. Nitrogen (> 99% pure) was used as the carrier/purge gas for both KI5 and H<sub>2</sub>S. The PCVD timing sequence consisted of a 3 s N<sub>2</sub> purge followed by a 5 s H<sub>2</sub>S exposure, another 3 s purge, and finally a 12 s KI5 exposure. The chamber pressure was maintained at 0.3 Torr during the KI5 and between 0.3 and 0.6 Torr during the H<sub>2</sub>S exposure. The chamber pressure during CVD depositions ranged between 0.7 and 0.9 Torr. For both processes, H<sub>2</sub>S was formed *in situ* by reacting Al<sub>2</sub>S<sub>3</sub> powder with water. The H<sub>2</sub>S gas was passed through a powder desiccant to reduce the residual water content to less than 1% of the H<sub>2</sub>S. A quadrupole mass spectrometer was used to monitor the purity of the H<sub>2</sub>S reaction gas and reaction byproducts.

A hydrophilic substrate with a suitable electron valence state was necessary for a successful Cu<sub>x</sub>S PCVD deposition. Depositions were attempted on Corning Glass, sol-gel deposited TiO<sub>2</sub>, sintered 100 nm TiO<sub>2</sub> nanoparticles, and sol-gel deposited ZnO. Of these substrates, only the 100 nm TiO<sub>2</sub> nanoparticles and sol-gel ZnO yielded Cu<sub>x</sub>S from the PCVD process. The PCVD films on ZnO and TiO<sub>2</sub> were very uniform across the 1 in. substrate. Simultaneous flowing of the

reaction gases for the CVD process yielded Cu<sub>2</sub>S films on all substrate types, independent of substrate temperature, due to a gas phase reaction of the precursor and H<sub>2</sub>S in the chamber. The CVD films were very nonuniform, forming only directly below the injectors, indicative of a gas phase reaction rather than a reaction at the substrate's surface. The nanostructured TiO<sub>2</sub> films were made by spin-casting a commercial solution of suspended TiO<sub>2</sub> nanoparticles (Solaronex<sup>®</sup>), annealing in a vacuum oven for 1 h at 110 °C, and sintering the film in air for 10 min at 450 °C. The ZnO sol-gel process was adapted from a process illustrated in detail by Lee *et al.*<sup>15</sup> Zinc acetate was dissolved in a mixture of 2-methoxyethanol and monoethanolamine at room temperature. The mixture was then stirred at 60 °C for 2 h. Films were then spin cast, and the solvent was evaporated on a hot plate for 10 min. The sol-gel films were then annealed in a vacuum at 110 °C for 1 h and sintered in a tube furnace in air for 1 h at 450 °C.

## III. RESULTS AND DISCUSSION

### A. Pulsed CVD results

In previous work using ALD with Cu(thd)<sub>2</sub> as the Cu precursor, a drop in the measured growth rate at the transition temperature (180 °C) distinguished two deposition regimes of Cu<sub>x</sub>S crystal phases.<sup>10</sup> The PCVD process used here with KI5 copper precursor produced a consistent composition and deposition rate within the temperature range of 150–400 °C (Fig. 1) when deposited on planar ZnO. The initial thickness of the ZnO layer was measured at a minimum of three locations using an atomic force microscope (AFM) and an edge of the ZnO film patterned with a stainless steel scribe. After CuS deposition, the combined Cu<sub>x</sub>S/ZnO thickness was measured again with an AFM within 1 mm of the previous scribes, and the Cu<sub>x</sub>S thickness was deduced from the difference. Approximate stoichiometry measurements were performed using energy dispersive x-ray spectroscopy (EDS) and x-ray photoelectron spectroscopy (XPS). Table I illustrates the XPS energies used to calculate stoichiometry, as well as the associated uncertainties. The Cu:S ratio was measured as 1.8 to 2.1 at all

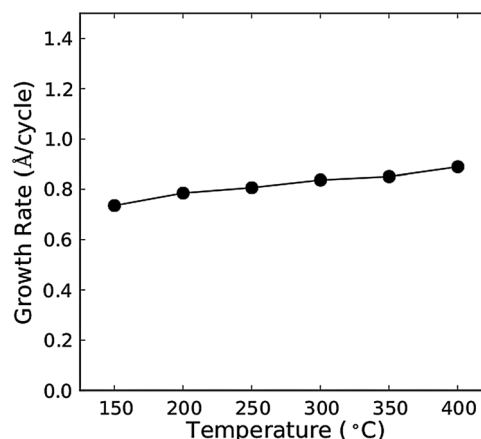


FIG. 1. Growth rate and substrate temperature using alternating pulses of H<sub>2</sub>S and precursor.

TABLE I. Typical XPS results used to determine the composition of PCVD Cu<sub>x</sub>S deposited at 400 °C in a porous matrix of TiO<sub>2</sub>.

Peak identity	Energy (eV)	Width (eV)	Area (eV)	Relative concentration
Cu 2p	932	2.62	373	67 ± 2%
S 2p	162	2.75	12	32 ± 6%

deposition temperatures, which is within the uncertainty of the EDS measurements due to the small amplitude of the sulfur peak. There are several different phases of Cu<sub>x</sub>S with stoichiometry between  $x=1.8$  to 2.1, and therefore EDS and XPS alone cannot be used to identify the chalcocite phase of the deposited film. The extended x-ray absorption fine structure (EXAFS) measurements described below are used to identify the specific phase of the Cu<sub>x</sub>S film.

Nanoporous films of sintered 100 nm TiO<sub>2</sub> nanoparticles were used to study the penetration of PCVD Cu<sub>x</sub>S. Figure 2 shows cross-sectional SEM images taken of sintered nanoparticle TiO<sub>2</sub> films with and without PCVD treatment. The second film, with 900 cycles of PCVD Cu<sub>x</sub>S deposited throughout, shows backfilling and a penetration depth of over 200 nm. The PCVD deposited film appears to show uniform coverage throughout the TiO<sub>2</sub> layer.

The Cu K-edge EXAFS data were collected at the Stanford Synchrotron Radiation Lightsource (SSRL) on beamline 10-2, using a Si (111) double monochromator detuned 50% in order to reduce harmonics. Slits with an approximate height of 0.5 mm gave an energy resolution of 1.3 eV. The

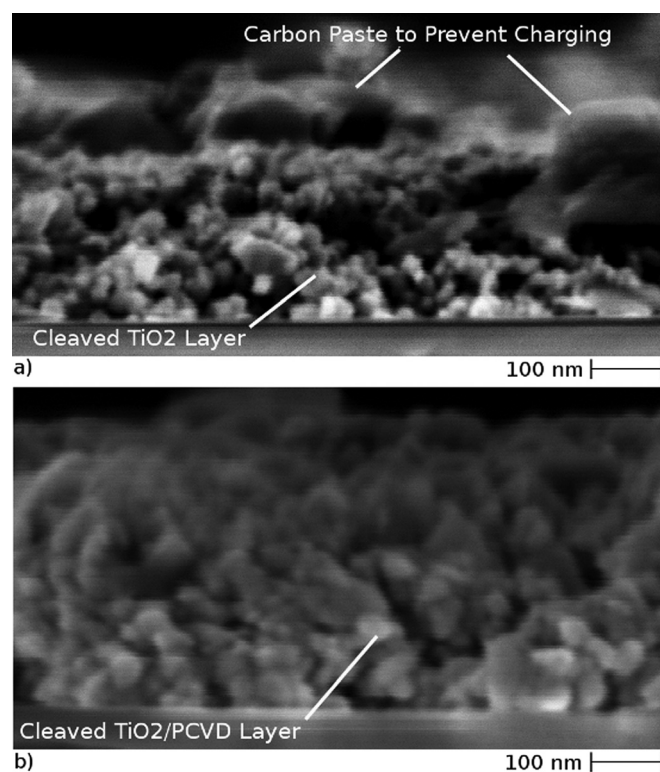


Fig. 2. Cleaved SEM cross section of a mesoporous TiO<sub>2</sub> film (a) before and (b) after Cu<sub>2</sub>S deposition. The porous TiO<sub>2</sub> film is successfully filled with PCVD Cu<sub>2</sub>S.

data were collected in fluorescence mode (13-element Ge detector) at a temperature of 6 K, with the x-ray polarization at either 10° or 80° relative to the film surface.

For these measurements, the Cu<sub>x</sub>S film was deposited into a mesoporous TiO<sub>2</sub> substrate with 1000 cycles (with an approximate thickness of 80 nm). The EXAFS data were reduced using standard techniques (RSXAP) [R1]. A Fourier transform window of 3.5–11.0 Å<sup>-1</sup> was used to transform the k-space data into r-space. The r-space plots show negligible variation between data collected for the two different polarization orientations, and in the rest of the analysis/discussion we discuss fits for only the 10° data set shown in Fig. 3(c).

The purpose of the EXAFS measurements was to determine whether the deposited PCVD films were Cu<sub>2</sub>S, as opposed to some other Cu<sub>x</sub>S phase, as no diffraction peaks were observable in the thin films formed inside the mesoporous TiO<sub>2</sub>. EXAFS data for bulk CuS and Cu<sub>2</sub>S were used in addition to the simulated data for several compounds (Cu<sub>1.7</sub>S, Cu<sub>1.94</sub>S, and CuS) in order to show how the r-space scans change with different amounts of copper present. The simulations were calculated using the known crystal structures, the FEFF8.2 code [R2], and a small overall broadening factor for the pair distribution functions,  $\sigma=0.06$  Å. In Fig. 3(a) we compare the EXAFS r-space plots for these

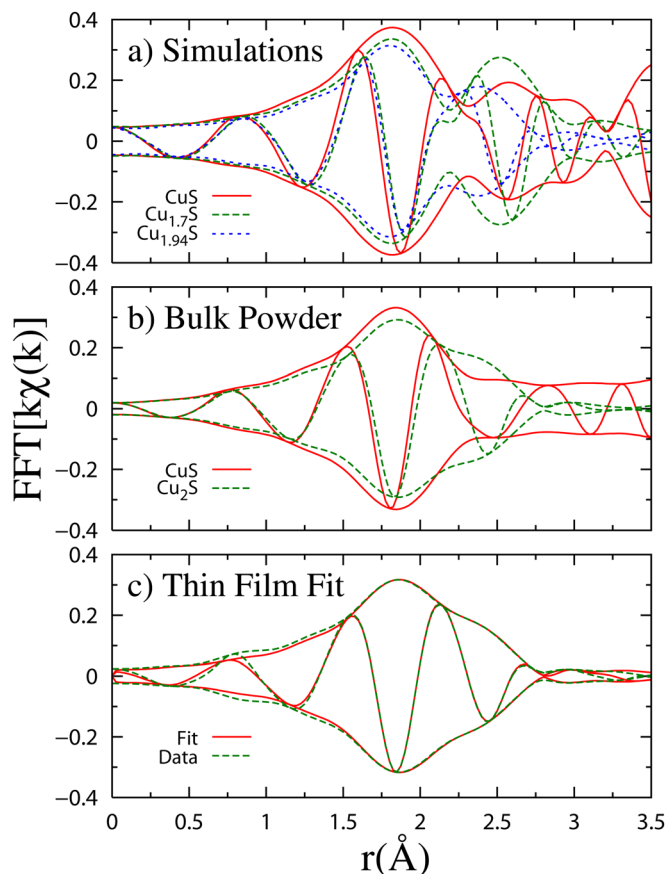


Fig. 3. (Color online) EXAFS r-space simulations for the CuS, Cu<sub>1.7</sub>S, and Cu<sub>1.94</sub>S phases (a) showing a large variation in spectra for small changes in stoichiometry. (b) EXAFS r-space data for bulk CuS and Cu<sub>2</sub>S. (c) Fits of the thin film data to a Cu<sub>2</sub>S structure.

simulations, and in Fig. 3(b) we compare the experimental data for the two bulk samples. At 6 K, Cu<sub>2</sub>S has a large distinct shoulder between 2 and 2.5 Å that corresponds to second neighbor copper atoms (Cu-Cu).

As the fraction of copper decreases from 2 to 1.94 to 1.7, this shoulder moves away from the main Cu-S peak (nearest neighbor S) located near 1.8 Å in the EXAFS plot. For Cu<sub>1.7</sub>S, the shoulder becomes a well defined second peak near 2.55 Å. In contrast, CuS has a significantly smaller shoulder (see Fig. 2(b)). These plots show that the various Cu<sub>x</sub>S phases can be easily differentiated.

Before fitting the PCVD film data, the bulk Cu<sub>2</sub>S data was fitted using two theoretical FEFF functions for Cu-S and Cu-Cu. The fit over the range of 1.5–2.6 Å was excellent. The PCVD thin film data were then fitted over the same r-range using the same FEFF functions as used to fit bulk Cu<sub>2</sub>S. The excellent fit (solid line) is compared with the data (dashed line) in Fig. 3(c). This result shows that the thin films deposited using PCVD are indeed Cu<sub>2</sub>S films.

In addition to the EXAFS measurements, which look at the entire film thickness, XPS measurements were used to isolate the composition at the surface of the PCVD deposited Cu<sub>x</sub>S films on TiO<sub>2</sub>. The electron binding energies of the copper 2p and sulfur 2p electrons and relative concentration values (Table I) are consistent with the Cu<sub>2</sub>S phase of the material.<sup>16</sup>

## B. CVD results

In order to study resistance and optical absorption across a wide range of film thicknesses, CVD films were deposited on Corning Glass. The CVD process was chosen over PCVD because a larger range of film thicknesses could be covered due to the higher film growth rate of CVD. Films over 100 nm were not feasible for PCVD due to the long deposition times required and depletion of the H<sub>2</sub>S source. Also, CVD film could be deposited directly on glass, which simplified the sheet resistance and optical absorption measurements. Films deposited via PCVD nucleated only on ZnO and porous TiO<sub>2</sub>. It should be noted that EXAFS and energy-dispersive x-ray spectroscopy (EDX) measurements show no

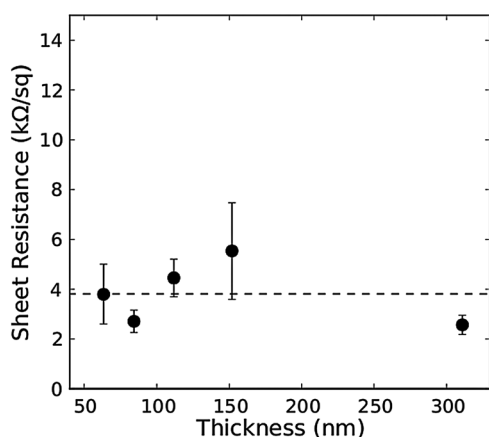


FIG. 4. Sheet resistance and thickness for CVD deposited Cu<sub>x</sub>S films showing the presence of a metallic layer at the glass–Cu<sub>x</sub>S interface.

discernible compositional differences between CVD and PCVD films. Figure 4 shows four-point sheet resistance measurements of CVD-deposited Cu<sub>2</sub>S films on glass plotted versus the film thickness. The sheet resistance is constant with the thickness, suggesting that a copper-poor material preferentially formed at the substrate–Cu<sub>x</sub>S boundary and effectively shorts out the Cu<sub>2</sub>S film that forms the bulk of the film. The resistivity estimated from this sheet resistance is consistent with some previous studies on Cu<sub>x</sub>S thin films, suggesting that *x* is in the range of 1.9–2.0.<sup>17–19</sup> Other studies, however, report a widely varying range of resistivity values for the Cu<sub>x</sub>S films, clouding the information required in order to isolate the specific material phase.<sup>12,20</sup> PCVD films deposited in the porous TiO<sub>2</sub> matrix had sheet resistances that were too high to measure.

Conventional transmission spectroscopy had an insufficient dynamic range to resolve the low absorption tail and indirect bandgap of the Cu<sub>x</sub>S films. Instead, photothermal deflection spectroscopy (PDS) was used to measure optical absorption. The PDS technique requires that the sample be placed in contact with a material with an index of refraction that is sensitive to temperature. Absorption by the sample creates a temperature gradient in this surrounding material, and absorption measurements are achieved by measuring the deflection of a laser beam that is passed through the surrounding material. Figure 5 contains the absorption data for films with thicknesses ranging between 63.3 and 310.8 nm deposited on Corning Glass via CVD. Cu<sub>x</sub>S films less than 100 nm appear to show a high absorption in the infrared region due to free carriers. This behavior is consistent with more metallic copper-poor crystal phases.<sup>19</sup> Films greater than 100 nm in thickness have distinguishable direct and indirect band gaps consistent with the copper-rich semiconducting crystal phases. Extrapolation of the absorption to the *x*-intercepts of the  $(\alpha h\nu)^2 \sim h\nu$  and  $(\alpha h\nu)^{1/2} \sim h\nu$  plots for the 310.8 nm film revealed a direct band gap of 1.8 eV and an indirect band gap of 1.2 eV. Chalcocite is reported to have an indirect band gap in the range of 1.05–1.21 eV and a

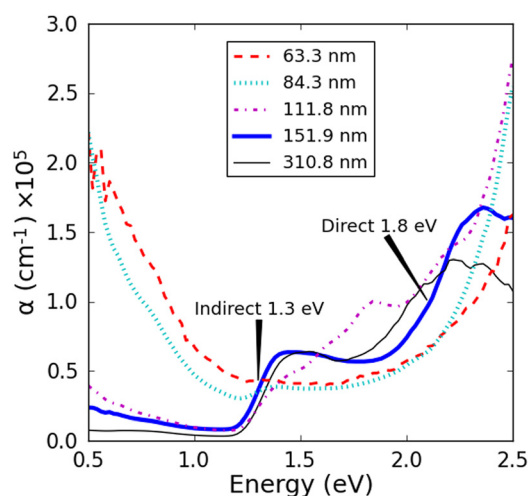


FIG. 5. (Color online) Optical absorption and thickness for a series of CVD deposited Cu<sub>2</sub>S films showing metallic behavior for films less than 100 nm thick and semiconducting Cu<sub>2</sub>S for films greater than 100 nm thick.

direct band gap of 1.7–1.8 eV.<sup>13,21</sup> The band gaps of copper-poor films are shifted higher than those of Cu<sub>2</sub>S because the removal of copper ions results in the removal of electrons from the top of the valence band.<sup>22</sup> CuS and Cu<sub>1.8</sub>S have been reported to have an indirect band gap of 1.55 eV, whereas Cu<sub>1.96</sub>S has an indirect band gap of 1.4 eV.<sup>8</sup> For x in the range of 1.935–1.955, Cu<sub>x</sub>S is reported to have a direct band gap of 1.3 eV.<sup>21</sup> Previous studies have also shown band gaps between 1.85 and 2.16 eV for x in the range of 1.89–1.94.<sup>20</sup>

#### IV. SUMMARY AND CONCLUSION

PCVD and CVD Cu<sub>x</sub>S materials were deposited using the KI5 copper-organic precursor and H<sub>2</sub>S gas. Consistent deposition rates in the temperature range of 150–400 °C and EXAFS analysis of the deposited films suggest that film composition is largely independent of the substrate temperature during the deposition process. EXAFS was used to investigate the average compositional analysis of the PCVD Cu<sub>x</sub>S films, and XPS was used to study the surface layer of the deposited films. The majority of the film composition appears to be largely Cu<sub>2</sub>S, but the planar resistivity measurements do not scale with film thickness and appear to be dominated by copper-poor states present in the film. Photo-thermal deflection spectroscopy was used to measure absorption at the surface of CVD Cu<sub>x</sub>S deposited on glass. The results indicate copper-rich phases for greater thicknesses, whereas thinner films appear to show metallic copper-poor behavior. It is proposed that absorption in the thinner films is dominated by a copper-poor film region located near the substrate boundary, whereas absorption in thicker films is dominated by a copper-rich phase located closer to the surface.

#### ACKNOWLEDGMENTS

This work was supported by the U.S. Department of Energy through DE-FG36-08GO18014 and the National

Science Foundation through DMR1006190. The EXAFS experiments were performed at SSRL (operated by the DOE, Division of Chemical Sciences, and by the NIH, Biomedical Resource Technology Program, Division of Research Resources).

- <sup>1</sup>K. Ernst, A. Belaidi, and R. K. Nenkamp, *Semicond. Sci. Technol.* **18**, 475 (2003).
- <sup>2</sup>C. Jezewski, W. A. Lanford, J. J. Senkevich, D. Ye, T. M Lu, and C. Jin, *Chem. Vap. Deposition* **9**, 305 (2003).
- <sup>3</sup>J. Bragagnolo, A. Barnett, J. Phillips, R. Hall, A. Rothwarf, and J. Meakin, *IEEE Trans. Electron Devices* **27**, 645 (1980).
- <sup>4</sup>A. Aldhafiri, G. Russell, and J. Woods, *Semicond. Sci. Technol.* **7**, 1052 (1992).
- <sup>5</sup>L. Reijnen, B. Meester, A. Goossens, and J. Schoonman, *Mater. Sci. Eng., C* **19**, 311 (2002).
- <sup>6</sup>G. Liu, T. Schulmeyer, A. Thissen, A. Klein, and W. Jaegermann, *Appl. Phys. Lett.* **82**, 2269 (2003).
- <sup>7</sup>M. Burgelman and H. Pauwels, *Electron. Lett.* **17**, 224 (1981).
- <sup>8</sup>M. T. S. Nair, L. Guerrero, and P. K. Nair, *Semicond. Sci. Technol.* **13**, 1164 (1998).
- <sup>9</sup>K. Chopra and S. Das, *Thin Film Solar Cells*, 1st ed. (Springer, New York, 1983).
- <sup>10</sup>L. Reijnen, B. Meester, A. Goossens, and J. Schoonman, *Chem. Vap. Deposition* **9**, 15 (2003).
- <sup>11</sup>L. Reijnen, B. Meester, F. de Lange, J. Schoonman, and A. Goossens, *Chem. Mater.* **17**, 724 (2005).
- <sup>12</sup>J. Johansson, J. Kostamo, M. Karppinen, and L. Niinisto, *J. Mater. Chem.* **12**, 1022 (2002).
- <sup>13</sup>A. B. F. Martinson, J. W. Elam, and M. J. Pellin, *Appl. Phys. Lett.* **94**, 123107 (2009).
- <sup>14</sup>J. A. Norman, M. Perez, S. E. Schulz, and T. Waechtler, *Microelectron. Eng.* **85**, 2159 (2008).
- <sup>15</sup>J. Lee, K. Ko, and B. Park, *J. Cryst. Growth* **247**, 119 (2003).
- <sup>16</sup>I. Nakai, Y. Sugitani, K. Nagashima, and Y. Niwa, *J. Inorg. Nucl. Chem.* **40**, 789 (1978).
- <sup>17</sup>J. Cardoso, O. Gomez-Daza, L. Ixtlilco, M. T. S. Nair, and P. K. Nair, *Mod. Phys. Lett. B* **15**, 774 (2001).
- <sup>18</sup>M. T. S. Nair and P. K. Nair, *Semicond. Sci. Technol.* **4**, 191 (1989).
- <sup>19</sup>I. Grozdanov and M. Najdoski, *J. Solid State Chem.* **114**, 469 (1995).
- <sup>20</sup>S. Couve, L. Gousskov, L. Szepessy, J. Vedel, and E. Castel, *Thin Solid Films* **15**, 223 (1973).
- <sup>21</sup>O. Madelung, *Semiconductors: Basic Data*, 2nd ed. (Springer, New York, 1996).
- <sup>22</sup>B. J. Mulder, *Phys. Status Solidi A* **13**, 79 (1972).